Soil Dynamics and Earthquake Engineering 130 (2020) 105971

Contents lists available at ScienceDirect

Soil Dynamics and Earthquake Engineering

journal homepage: http://www.elsevier.com/locate/soildyn

Prediction of seismic compression of saturated sand considering the ground motion characteristics and variable permeability

Guang-yun Gao [a,b,*], Wei Xie [a,b], Jian Song [c], Yu Wang [d]

[a] College of Civil Engineering, Tongji University, Shanghai, 200092, China
[b] Key Laboratory of Geotechnical and Underground Engineering of Ministry of Education, Tongji University, Shanghai, 200092, China
[c] Key Laboratory of Ministry of Education for Geomechanics and Embankment Engineering, College of Civil and Transportation Engineering, Hohai University, Nanjing, 210098, China
[d] Department of Civil and Environmental Engineering, The University of Auckland, Auckland, 1010, New Zealand

ARTICLE INFO

Keywords:
Permeability coefficient
Seismic motion characteristics
Seismic compression of saturated sand
Relative density
OpenSees
Numerical analysis

ABSTRACT

A one dimensional shear beam numerical model was firstly established to calculate the seismic compression in free-field site of saturated sand by using OpenSees program. Based on the established model, the influence of permeability coefficient on the liquefaction-induced settlement of saturated sand was investigated by introducing a variable permeability coefficient model. The modified model was verified by comparison with results from centrifuge model test. The correlation between seismic compression and seismic load parameters was studied, and a velocity spectrum intensity (VSI) based prediction function was proposed to estimate the compression of saturated sand by considering both the characteristics of seismic motion and the sand properties. The results show that the modified variable permeability model significantly improves the accuracy of the simulation results. Direction of seismic motion has a significant effect on the seismic compression and excess pore water pressure of sand, and the simplification of using one-dimensional load in a certain direction to represent the two-dimensional loads underestimates the seismic compression of sands. The proposed VSI-based prediction function provides a means for estimating seismic compression of saturated sand, and the prediction accuracy improves with increasing the relative density of sand.

1. Introduction

Liquefaction of saturated sand is a common phenomenon in earthquakes, which often leads to lateral deformation, seismic compression and sand boils. Seismic compression of saturated sandy deposits was observed in almost all strong earthquakes. For horizontal free-field sand sites, seismic compression is mainly caused by volumetric strain, and results in ground settlement. Numerical simulation and laboratory tests are widely used to study the deformation of saturated sand during earthquake loading. However, it is found that the seismic compression of saturated sand determined through numerical simulation is smaller than that of field observations and model tests [1,2]. This is the result of failure to capture the complex behaviors of liquefaction of saturated sands using the current constitutive model in the numerical simulation (e.g., Andrianopoulos et al. [1], Elgamal et al. [3], Boulanger et al. [4], Zhang et al. [5]).

As a matter of fact, this phenomenon can be theoretically explained by the settlement mechanism of saturated sand. Jafarzadeh and Yanagisawa [6] conducted a series of unidirectional shaking table tests to study the settlement of saturated sand columns in various conditions, and they found that the average permeability coefficient during seismic excitation is 5–6 times greater than its static (pre-shaking) value. Arulanandan and Sybico [7] attributed the increase of the permeability coefficient of saturated sands in liquefaction state to the changes of particle fabric. The contacts between soil particles are weaken during liquefaction, which results in more flow channels for the pore water and leads to the increase of permeability coefficient of the sand. Shahir et al. [8] found that the generation and seepage of excess pore water pressure exist simultaneously under seismic loads, and the coupling of accumulation and dissipation of pore pressure affects the seismic compression of saturated sand. Later, it is found that a variable permeability model used to simulate the centrifuge test can obtain more accurate results [9]. Rahmani et al. [10] considered the pore pressure accumulated non-linearly during seismic shaking, and modified the variable

* Corresponding author. Department of Geotechnical Engineering, Tongji University, Shanghai, 200092, China.
E-mail addresses: gaogy@tongji.edu.cn, gaoguangyun@263.net (G.-y. Gao).

https://doi.org/10.1016/j.soildyn.2019.105971
Received 5 June 2019; Received in revised form 6 November 2019; Accepted 11 November 2019
Available online 18 November 2019
0267-7261/

permeability model parameters. A large number of model tests and field observations showed that, seismic compression of saturated sand mainly occurs during the loading process, and the liquefaction will increase the final seismic compression of sand [11]. The previous studies indicated that the seepage effect in the vibration process cannot be ignored, and the accuracy of numerical simulation can be improved by using appropriate models to describe the seepage of pore water during earthquakes.

In addition, the seismic load is a random, irregular cyclic loading. In order to simplify the analysis, a single horizontal component was widely used in studies of sand compression. However, ground motion characteristics are significantly affected by the directionality, and the use of unidirectional ground motion component cannot represent the real earthquake loading (e.g., Bradley and Baker [12]). Many researches showed that ground motion directionality has significant influence on the settlement of sandy deposits and seismic displacement of slopes (e.g., Nie et al. [13], Boore [14], García et al. [15], Song et al. [16,17]). Moreover, characteristics of ground motion are commonly represented by various Intensity Measures (IMs), such as peak ground acceleration (PGA), peak ground speed (PGV), Arias intensity (Ia) and spectral acceleration (Sa) (e.g., Ishihara and Yasuda [18], Riddell and Eeri [19], Athanatopoulou et al. [20]). Thus, it is valuable to explore the correlation between the seismic compression of saturated sand and different ground motion IMs.

A large number of studies have been carried out to understand seismic compression and to predict its magnitude. On the one hand, Shahnazari and Towhata [21], Whang and Stewart [22] and Stamatopoulous et al. [23] studied the settlement characteristics of sand with different compositions through a series of experiments. However, most of the studies were limited to the seismic compression based on one component of horizontal earthquake motions. On the other hand, several approaches for predicting the severity of seismic compression were proposed (e.g., Pyke et al. [24], Tokimatsu and Seed [25], Duku et al. [26], Ghayoomi et al. [27], Lasley et al. [28]). The US Pacific Earthquake Engineering Research Center (PEER) proposed a performance-based earthquake engineering design theory (PBEE), where seismic compression and ground motion characteristics were directly linked based on correlation analysis between IMs and structural engineering demand parameters (EDP) [29]. However, the previous methods to estimate seismic compression were mainly for sites with unsaturated soils, and researches carried out on seismic compression of saturated sand did not consider the combined effect of ground motion characteristics and variable permeability.

In this paper, a numerical simulation of seismic responses of free field sites with saturated Fujian sand was carried out on OpenSees platform. The influence of permeability coefficient on liquefaction and seismic compression was discussed, and suitable parameters of the variable permeability coefficient model for Fujian sand were proposed to improve accuracy of the numerical test. The effects of ground motion dimension and directionality on sand compression were studied. Particular attentions have been paid to different ground motion intensity measures and their relation to seismic compression, as well as the effect of relative density of sand. On this basis, a prediction function of seismic compression of saturated sand was proposed.

2. Constitutive model

The constitutive model proposed by Wang et al. [2] operating within the framework of bounding surface plasticity [30] can reproduce small to large deformation in the pre-to post-liquefaction regime. Principles of critical state soil mechanics were incorporated into the model by introducing the state parameters ψ into plastic modulus and shear-induced volumetric strains [31]:

$$\psi = e - e_c \tag{1}$$

in which e and e_c are current void ratio and critical void ratio corresponding to the existing confining stress, respectively. e_c can be derived from the following energy equation [31]:

$$e_c = e_0 - \lambda_c (P_c/P_{at})^{\xi} \tag{2}$$

where P_c represents existing confining stress; P_{at} is the standard atmospheric pressure; e_0 is the void ratio at $P_c = 0$; λ_c and ξ are model parameters.

The model assumes that the volumetric strain caused by the mean effective stress is elastic, and the total volumetric strain ε_v caused by shear stress is completely plastic, which can be expressed as [31]:

$$\varepsilon_v = \varepsilon_v^e + \varepsilon_v^p = \varepsilon_{vc} + \varepsilon_{vd} = \varepsilon_{vc} + \varepsilon_{vd,ir} + \varepsilon_{vd,re} \tag{3}$$

where ε_v^e and ε_v^p are elastic volumetric strain and plastic volumetric strain; ε_{vc} and ε_{vd} denote the volumetric strain caused by the mean effective stress and the volumetric strain caused by dilatancy. $\varepsilon_{vd,ir}$ and $\varepsilon_{vd,re}$ represent the irreversible and reversible parts, respectively. The total strain rate can be expressed as [31]:

$$\dot{\varepsilon} = \frac{1}{2G} p' \dot{\mathbf{r}} + \left(\frac{1}{2G}\mathbf{r} + \frac{1}{3K}\mathbf{I}\right)\dot{p} + \left(\mathbf{m} + \frac{D}{3}\mathbf{I}\right)\langle L \rangle \tag{4}$$

in which $p' = \mathrm{tr}(\boldsymbol{\sigma})/3$, $\boldsymbol{\varepsilon}$, $\boldsymbol{\sigma}$ and $\mathbf{r} = s/p'$ represent mean effective stress, strain tensor, the effective stress tensor and the deviatoric stress ratio tensor, respectively; L is the plastic loading intensity; $\mathbf{m}$ is the deviatoric strain flow direction; D is total dilatancy rate; G and K are the elastic shear modulus and bulk modulus, respectively.

The failure surface, maximum stress ratio surface (boundary surface) and dilatancy surface used in the model are shown in Fig. 1, which are defined as [2]:

$$f_c(\boldsymbol{\sigma}) = \eta - M g(\theta) = 0 \tag{5}$$

$$f_m(\boldsymbol{\sigma}) = \eta - M_m g(\theta) = 0 \tag{6}$$

$$f_d(\boldsymbol{\sigma}) = \eta - M_d g(\theta) = 0 \tag{7}$$

in which $\eta = q/p'$ and $q = \sqrt{\frac{3}{2}\mathbf{s} : \mathbf{s}}$ represent generalized shear stress ratio and deviatoric stress invariant; $\mathbf{s} = \boldsymbol{\sigma}\text{-}p'\mathrm{I}$ is the deviatoric stress tensor, $\mathbf{I}$ being the rank two identity tensor; M denotes critical stress ratio; θ is the Lode angle and $g(\theta)$ is the plastic potential function; $M_d = M \cdot \exp(-n^b \psi)$ represent the peak mobilized stress ratio at triaxial compression, n^b is plastic modulus parameter; M_m is the historical maximum stress ratio, which will be increased when the current stress ratio exceeds the peak value of M_d.

Within the framework of the boundary surface model, both of the plastic modulus H and the total dilatancy rate D are related to the

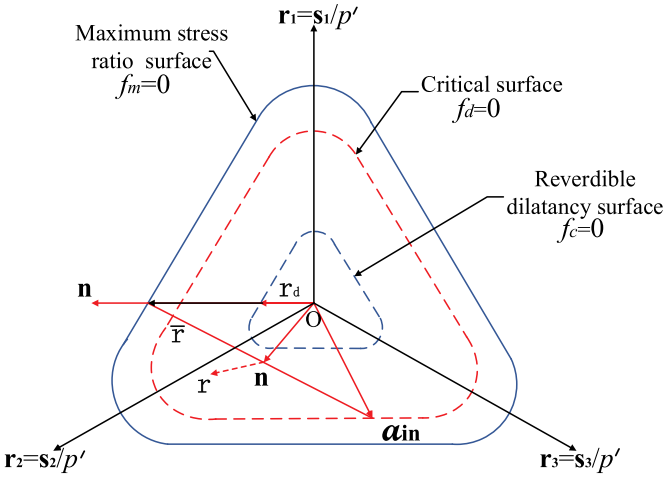

Fig. 1. Mapping rules of the model [2].

distance between the boundary surface and the dilatancy surface. H is defined as follows:

$$H = \frac{2}{3} hg(\bar{\theta}) G \exp(-n^p \psi) \left[\frac{M \exp(-n^b \psi)}{M_m} \left(\frac{\bar{\rho}}{\rho} \right) - 1 \right] \tag{8}$$

where h is a model parameters; n^p is a model constant; . is the distance between the projection center $\boldsymbol{\alpha}_{\mathbf{in}}$ and the image stress ration**r**, and ρ is the distance between the projection center $\boldsymbol{\alpha}_{\mathbf{in}}$ and the current stress reversal ration **r**, as shown in Fig. 1.

The constitutive model is currently integrated into the open source finite element platform OpenSees. There are fourteen parameters required by the model which can be obtained by a series of laboratory tests. The specific parameters of Fujian sand used in this paper are listed in Table 1, and their definitions are detailed in Ref. [2].

3. Modification of model parameters and validation of centrifuge test

3.1. Permeability coefficient model

The variable permeability coefficient model, as shown in Fig. 2, proposed by Shahir et al. [9] properly captured the changes in permeability during and after earthquake loading. This relationship between the permeability coefficient k and excess pore water pressure ratio r_u (defined as the ratio of excess pore water pressure to the initial vertical effective stress of soil) is expressed as follows [9]:

$$\frac{k}{k_0} = \begin{cases} 1 + (\alpha - 1) r_u^{\beta_1} & \text{during pore water pressure build up phase } (r_u < 1) \\ \alpha & \text{during liquefation state } (r_u = 1) \\ 1 + (\alpha - 1) r_u^{\beta_2} & \text{during pore water pressure dissipation phase } (r_u < 1) \end{cases} \tag{9}$$

where k_0 is initial permeability coefficient; k denotes permeability coefficient during different stages before and after liquefaction; α, β_1 and β_2 are model parameters detailed in Ref. [9].

It can be seen that the value of permeability coefficient in liquefaction stage is α times larger than that in the initial state. β_1 and β_2 are parameters describing the accumulation rate of excess pore pressure before liquefaction and dissipation rate of pore pressure after liquefaction, respectively. Shahir et al. [8] simulated the centrifuge test of Nevada sand to determine the model parameters as $\alpha = 20$, $\beta_1 = 1.0$, $\beta_2 = 8.9$. Then Shahir et al. [9] pointed out that the value of the permeability coefficient in the liquefaction stage increased 20 times than that in the initial state, and the model parameters were further modified as $\alpha = 10$, $\beta_1 = 2.0$ and $\beta_2 = 10.0$.

Based on the two sets of model parameters ($\alpha = 20$, $\beta_1 = 1.0$, $\beta_2 = 8.9$ and $\alpha = 10$, $\beta_1 = 2.0$, $\beta_2 = 10.0$) and the results of the constant permeability coefficient model, the influence of the permeability coefficient model on the seismic compression is analyzed and the parameters of the Fujian sand permeability coefficient model is modified by parameter analysis. On this basis, six sets of ground motion acceleration time history were selected from the NGA West-2 database [32] as the input loads in numerical analysis. Effects of the earthquake loading characteristics such as ground motion dimension, directionality and intensity measures on the seismic compression were analyzed in detail. The sequence of ground motions are shown in Table 2, and each sequence of seismic records include two horizontal components and one vertical component.

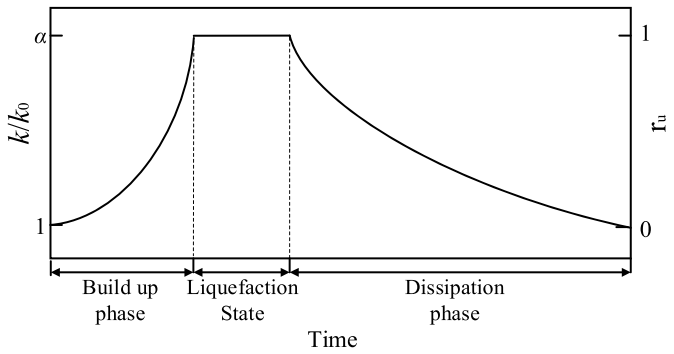

Fig. 2. Schematic of permeability coefficient function [9].

3.2. Centrifuge model test

The numerical simulation of free-field seismic compression is based on the centrifuge model test of Fujian Sands carried out by Liang and Zhou [33]. The scaling factor of the test was 50 and the depth of the model was 40 cm (20 m in prototype). The sample was prepared by air pluviation method and saturated by silicone oil whose viscosity was 50 times of that of water under vacuum condition. The relative density was 72.9% after consolidation under 50g. The test model was unidirectionally excited with different maximum acceleration (0.118g and 0.243g) of Deyang seismic wave in the Wenchuan earthquake, and the original waveform is shown in Fig. 3. The first loading amplitude is small so that no liquefaction is induced, and the observed ground surface settlement is only about 5 mm in prototype. Hence only the second loading with an amplitude $a_{max} = 0.243$g is performed in the numerical simulation. The physical and mechanical properties of Fujian sand in the numerical test are shown in Table 3. As the physical parameters of the sand are similar and the sample preparation method is the same, the constitutive model parameters proposed by Wang et al. [2] was used to simulate seismic compression.

The empirical relationship between permeability coefficient and void ratio proposed by Taylor [34] is:

$$k = C \frac{e^m}{1 + e} \tag{10}$$

where C is a parameter related to soil properties; m denotes a parameter of the empirical index, which is generally taken as 3. The relationship between the void ratio and D_r is:

$$D_r = \frac{e_{max} - e}{e_{max} - e_{min}} \tag{11}$$

where e_{max} and e_{min} are maximum void ratio and minimum void ratio of Fujian sand, respectively. The experimental results show that the permeability coefficient is $k = 2.056 \times 10^{-3}$ cm/s when the relative density of Fujian sand is $D_r = 55\%$. Thus, based on Eqs. (10) and (11), the permeability coefficient of Fujian sand is $k = 1.652 \times 10^{-3}$ cm/s when $D_r = 72.9\%$.

A soil column model to simulate the dynamic response of saturated sand has been successfully used by Phillips et al. [35]. On this basis, a one dimensional shear beam numerical model for predicting the free-field seismic compression of saturated sand was established in this paper. Unidirectional excitation of the experimental model corresponding to the site prototype in OpenSees is shown in Fig. 4. The assumption of numerical model is that the sand layer is homogeneous,

Table 1
Model parameters of Fujian sand [2].

Parameter	G_0 (MPa)	κ	h	M	$d_{re,1}$	$d_{re,2}$	d_{ir}	α	$\gamma_{d,r}$	n^b	n^d	λ_c	e_0	ξ
Value	200	0.006	1.7	1.3	0.45	30	0.6	40	0.05	1.1	8.0	0.023	0.837	0.7

Table 2
Input earthquake ground motions.

Sequence (RSN)	145	184	320	547	4121	4127
Location and year	Coyote Lake, 1979	Imperial Valley-06, 1979	Mammoth Lakes-10, 1981	Chalfant Valley-01, 1986	Parkfield-02 CA, 2004	Parkfield-02 CA, 2004
Peak ground acceleration (g)	0.247	0.481	0.162	0.272	0.209	0.187

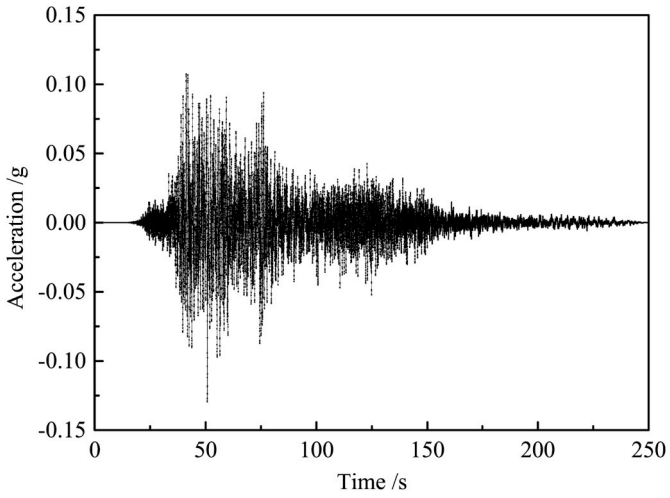

Fig. 3. Initial Deyang seismic wave.

isotropic, and the D_r value is constant throughout the soil layer. Due to the symmetry of the free field, the model mesh consisted of 20.0 cube elements with a side length of 1.0 m, and a three-dimensional fully coupled unit BrickUP [36] was used. Considering the influence of the layered shear box in the centrifuge test, the same layer nodes were bounded in three directions, and the bottom nodes were constrained in all directions. The bottom and two lateral sides of the model are undrained, and the top surface was drained to maintain the excess pore pressure at zero. Numerical analysis includes three stages, i.e., calculation of the geostatic stresses, dynamic response analysis of seismic load and reconsolidation analysis. In order to incorporate the variable permeability coefficient model of Eq. (9), the permeability coefficient of each element was updated according to the excess pore water pressure ratio at differential depth in the calculation.

3.3. Modification of permeability coefficient

Considering the results of Refs [8,9], this study set $\beta_1 = 1.0$ and $\beta_2 = 10.0$, and α values are taken as 10, 20 and 25, respectively. The value of $\alpha = 10$ means that the permeability coefficient of sand increases to 10 times of the initial value in the liquefaction stage. The time-history curve of seismic compression in saturated sand field under three kinds of model parameters were analyzed, and the result of seismic compression with a constant increased permeability coefficient model ($k = 10k_0$) was compared, as shown in Fig. 5. As can be seen from Fig. 5, most of the settlement occurs during the loading process (from about 30s to 200s), which is consistent with the results of centrifuge model test [33]. The reason for this phenomena is that the average permeability coefficient of sand is several times greater during seismic excitation than its static (pre-shaking) value, which can result in that the volume of drained water during shaking is larger than the reconsolidation process. In addition, the compression accumulation and the final settlement increased with increasing of α. For the case of $k = 10k_0$, the final compression value is smaller than that corresponding to $\alpha = 10$, 20 and 25. The simulation result is 260 mm when $\alpha = 25$, which is the closest to the 275 mm of centrifuge test result [33].

Fig. 6 shows the r_u development curve at depths of 3.25 m and 17.00 m for both constant increased permeability coefficient model

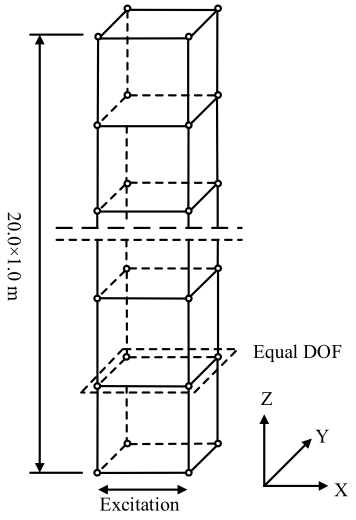

Fig. 4. Schematic of the simulation model.

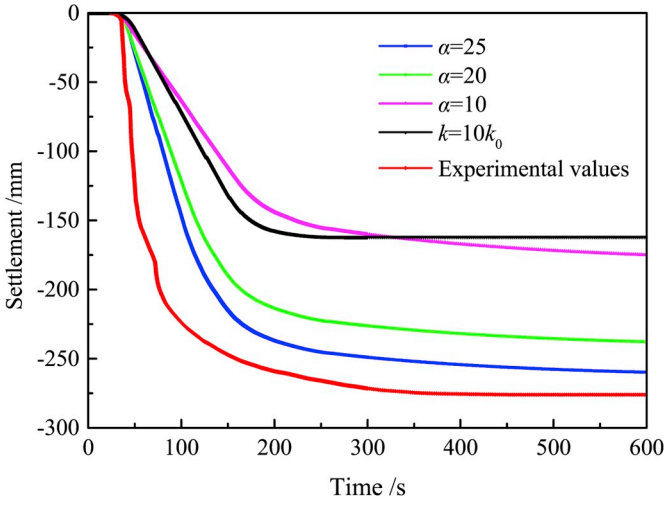

Fig. 5. Variation of settlement versus time for different α.

Table 3
The physical and mechanical properties of Fujian sand [33].

Parameter	G_s	e_{max}	e_{min}	D_{50}/mm	D_{30}/mm	D_{10}/mm	C_u	C_c	ϕ/°
Value	2.622	0.943	0.6	0.16	0.14	0.10	1.7	0.96	39

($k = 10k_0$) and variable permeability coefficient models (i.e., $\alpha = 10$, 20 and 25). It can be seen that the excess pore pressure ratio curve is significantly different for constant increase permeability coefficient model and variable permeability coefficient models. The rate of pore pressure accumulation in the early stage for $k = 10k_0$ is relatively slower than the case of $\alpha = 10$, 20 and 25. For the case of $k = 10k_0$, the pore water pressure dissipation is fast and the settlement curve is flat in the later stage. For the case of $\alpha = 10$, 20 and 25, the pore pressure dissipates slowly and the re-consolidation stage lasts for a long time. The comparison shows that the variable permeability coefficient model is more consistent with the experimental results. In addition, for the variable permeability coefficient models, the excess pore pressure ratio decreases with the increase of α in the pore water pressure dissipation stage.

Based on the above comparative analysis, it can be seen that the constant permeability coefficient model cannot reflect the real situation of excess pore water pressure and settlement development of saturated sand under seismic loading. The numerical simulation results obtained by using the variable permeability coefficient model generally agree well with the experimental results when $\alpha = 25$. Therefore, the value of parameter α is set as 25 in the following simulations to evaluate the free field settlement of saturated Fujian sand.

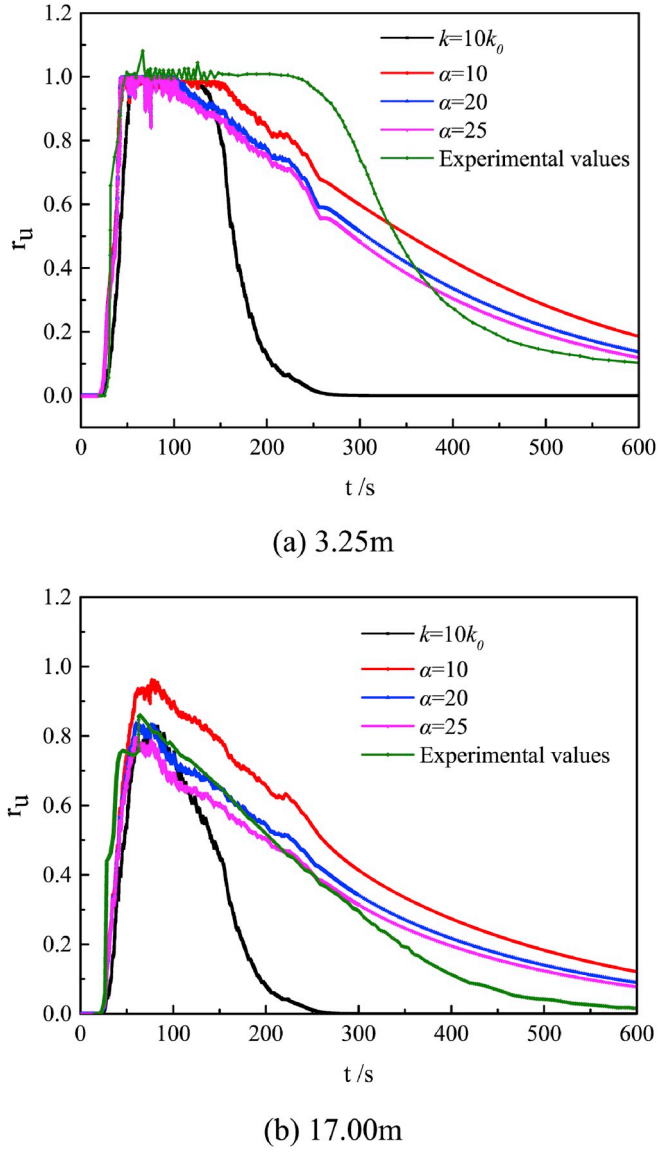

Fig. 6. Variation of excess pore water pressure ratio r_u versus time for $k = 10k_0$ and $\alpha = 10$, 20, 25 at depths of 3.25 m and 17.00 m: (a) 3.25 m and (b) 17.00 m.

Fig. 7 shows the variation of settlement factor and excess pore pressure factor at the depth of 17.00 m when $\alpha = 25$, $\beta_2 = 10.0$ and β_1 is taken as integers from 1.0 to 5.0. The settlement factor and the excess pore pressure factor are defined as the ratio of the simulated value of the final settlement to the experimental value and the ratio of the simulated value of the maximum excess pore pressure at a certain depth to the experimental value, respectively. One can see from Fig. 7, the final settlement decreases with increasing of β_1, and the maximum pore pressure of the unliquefied fraction increases with increasing of β_1. These variations of both settlement factor and excess pore pressure factor are consistent with those described by Shahir et al. [8]. Based on the analysis results of Shahir et al. [9], β_1 varies between 1.0 and 3.0. In this paper, the obtained simulation results are more accurate for $\beta_1 = 2.0$.

The parameter of β_2 mainly controls the rate of excess pore pressure dissipation after liquefaction. As excess pore pressure in the dissipation stage increases with the increase of β_2 [8], the reasonable β_2 can be determined by analyzing the excess pore pressure factor of the pore pressure in dissipation stage. The rate of pore pressure dissipation is slower than that of accumulation (i.e., $\beta_2 > \beta_1$). By setting $\alpha = 25$ and $\beta_1 = 2.0$, the variation of excess pore pressure factor at 10.00 m for different β_2 in 200–600s is shown in Fig. 8. It can be seen that the excess pore pressure factor increased with increasing of β_2, which is in accordance with the results of Shahir et al. [9]. The excess pore pressure factors are closer to 1.0 for $\beta_2 = 10.0$ in 200–350s, which is also consistent with the results of Shahir et al. [9]. Base on the above analysis, the parameters of the variable permeability coefficient of Fujian sand can be redefined as: $\alpha = 25$, $\beta_1 = 2.0$ and $\beta_2 = 10.0$.

3.4. Calculation result verification

The modified parameters are applied to simulation of a centrifuge experiment, and the numerical results are shown in Fig. 9. As can be seen from Fig. 9, the settlement of numerical simulation are smaller than that of the experimental values. And the simulation results using the variable permeability coefficient model is closer to the experimental values than that using the constant permeability coefficient model.

The development curves of computed and measured values of excess pore water pressure ratio are depicted in Fig. 10. As shown in Fig. 10, the numerical results of the two permeability models at depth of 10.00 m indicate that liquefaction occurred during the loading process. In the process of pore pressure dissipation, the pore pressure ratio development curves at depths of 10.00 m and 17.00 m show that the velocity of pore pressure dissipation for the variable permeability coefficient model is slightly smaller than that of experimental value, which is opposite to

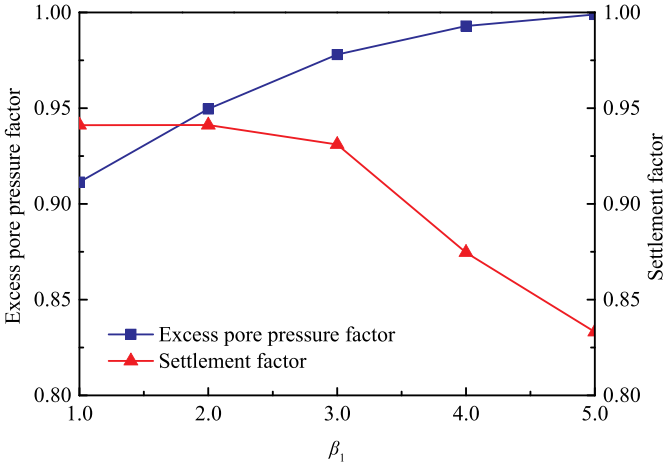

Fig. 7. Variation of settlement factor and excess pore pressure factor change with β_1 at depth of 17.00 m.

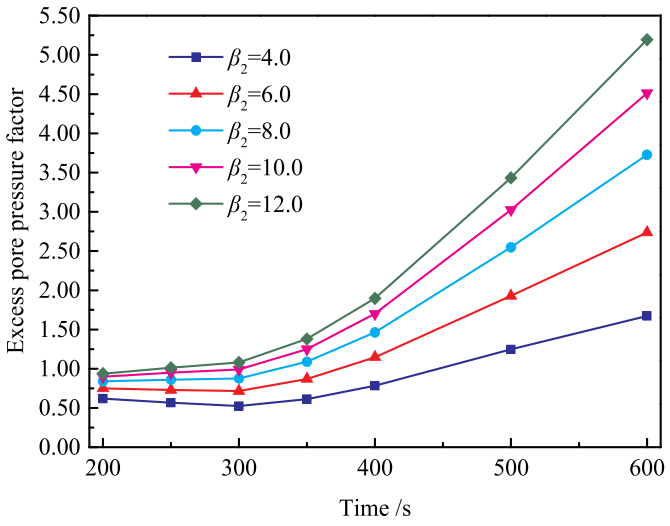

Fig. 8. Excess pore pressure factor change with time for different β_2 at depth of 10.00 m.

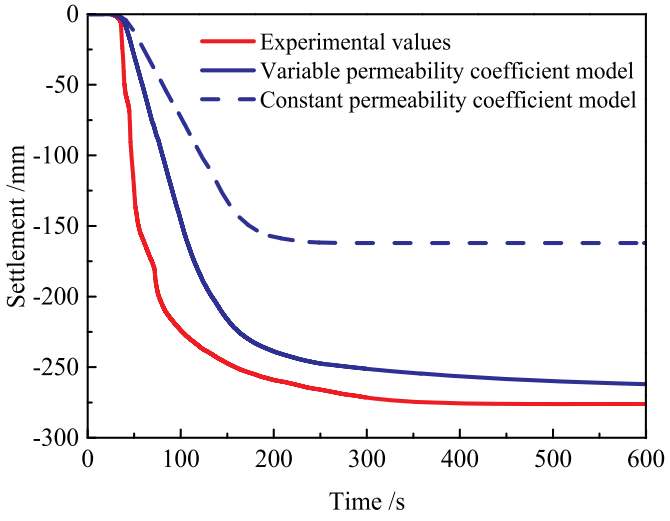

Fig. 9. Comparison of settlement change with time for different evaluation method.

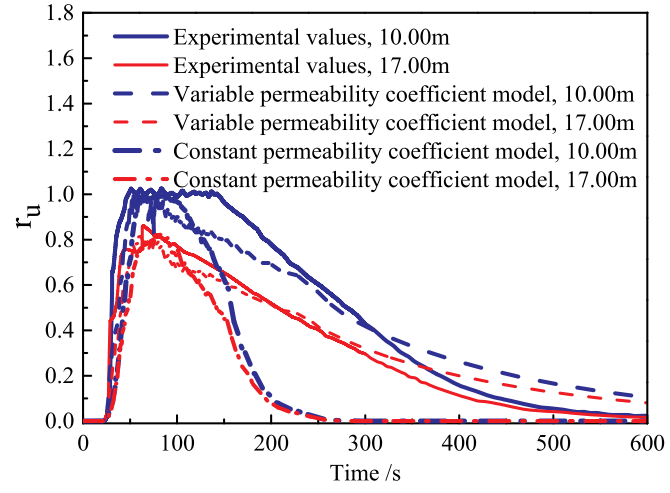

Fig. 10. Comparison of excess pore water pressure ratio r_u change with time for different evaluation methods and depths.

the constant permeability coefficient model.

Fig. 11 presents the variation of excess pore pressure factor (defined as in Fig. 7) of the variable permeability coefficient model and the constant permeability coefficient model. It can be seen from Fig. 11 that the excess pore pressure simulation results of the variable permeability coefficient model are in good agreement with the experimental values (i.e., the excess pore pressure factor is close to 1.00) in the 300s period, which are progressively larger than experimental values after 300s. In general, compared with the constant permeability coefficient model, using variable permeability model significantly improves the accuracy of the numerical simulation.

4. Results and analysis

4.1. Effect of input ground motion dimension on seismic compression

The recorded earthquake ground motion RSN145 was selected to explore the influence of ground motion dimension on seismic compression of saturated sand. The results of pore pressure and seismic compression subjected to one-dimensional (X-direction or Y-direction) and two orthogonal horizontal (XY-direction) earthquake loading were analyzed, and the difference between the two loading manners is discussed.

Fig. 12 shows the excess pore pressure ratio curves of saturated sand subjected to the two kinds of loading method (i.e., one-dimensional loading and two-dimensional loading) in the horizontal direction at depths of 2.00 m and 20.00 m. As can be seen from Fig. 12, the excess pore pressure of the sand subjected to two orthogonal horizontal loads are larger than that subjected to unidirectional horizontal seismic load. In addition, the excess pore water pressure ratio at depth of 2.00 m is larger than that at depth of 20.00 m under the same loading manner, which indicates that the excess pore water pressure ratio decreases with the increase of depth.

Fig. 13 shows the settlement time histories of saturated sand subjected to each of the horizontal components of motion separately and then simultaneously at ground surface. As shown in Fig. 13, the seismic compression of the sand subjected to two orthogonal horizontal loads are larger than that subjected to unidirectional horizontal seismic load, meanwhile, it is smaller than the sum of the seismic compression of the two unidirectional loads and the double of any one of them. Therefore, simplifying the seismic compression induced by two dimensional seismic loads as the double of that caused by unidirectional horizontal seismic load [24] for Fujian sand would result in overestimations.

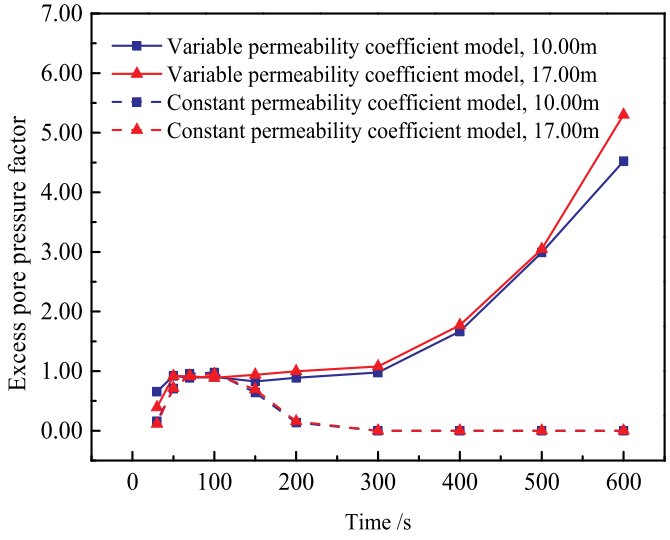

Fig. 11. Excess pore pressure factor change with time for different evaluation methods and depths.

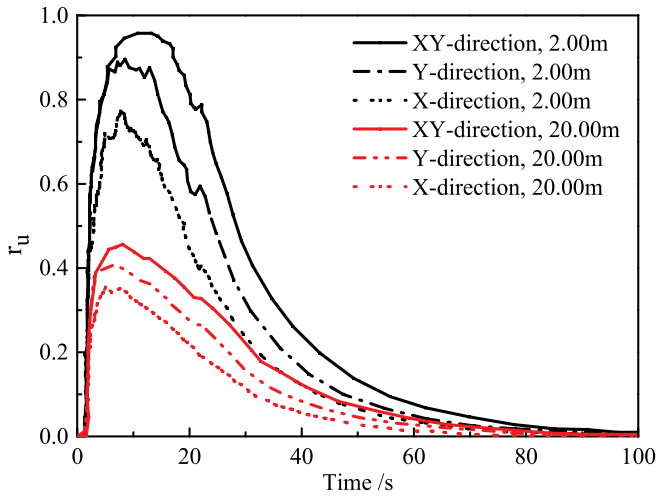

Fig. 12. Time history of the excess pore pressure ratio at depths of 2.00 m and 20.00 m.

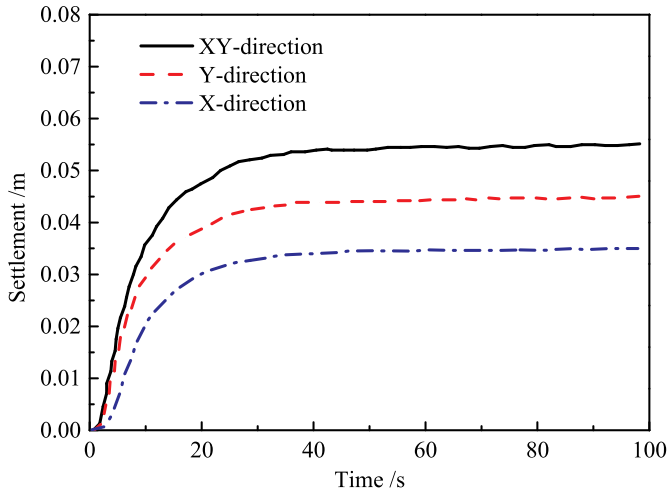

Fig. 13. Comparison of settlement time histories of saturated sand subjected to each of the horizontal components of motion separately and simultaneously at ground surface.

4.2. Effect of ground motion directionality on seismic compression

Based on Refs. [37–40], 17 IMs were used to describe the characteristics of ground motion in this paper, as shown in Table 4. The definition of each parameter can be found in Riddell et al. [19]. To capture the effects of the direction angle on seismic compression, a formulation proposed by Boore [14] was used to calculate the seismic acceleration time history in each direction, which can be expressed as Eq. (12):

$$a_{ROT}(t;\varphi) = a_1(t)\cos(\varphi) + a_2(t)\sin(\varphi) \tag{12}$$

where $a_1(t)$ and $a_2(t)$ are two orthogonal acceleration time history in horizontal direction of the original seismic record, respectively; φ represents the direction angle, which rotates from 0° to 175° on horizontal plane with a gradient of 5°. $a_{ROT}(t;\varphi)$ denotes the seismic acceleration component in the φ direction, and it was used as a seismic input load to simulate seismic compression of saturated sand with different relative densities.

The seismic compression is evaluated for unidirectional horizontal seismic load in different direction and for the bi-directional horizontal seismic load as well. The seismic compression ratio is defined as the ratio of the seismic compression caused by the seismic load component in a certain direction to the seismic compression generated by the bi-directional horizontal seismic load.

Table 4
Intensity measures of seismic waves.

Serial number	Ground-motion intensity parameters (IMs)
1	Peak ground acceleration, PGA
2	Peak ground speed, PGV
3	Peak ground displacement, PGD
4	Effective strong ground motion duration, D
5	Peak ground speed/Peak ground acceleration, V_{max}/A_{max}
6	Root mean square acceleration, RMS_a
7	Root mean square velocity, RMS_v
8	Root mean square displacement, RMS_d
9	Arias intensity, I_a
10	Cumulative absolute velocity, CAV
11	Filtered cumulative absolute velocity, CAV_5
12	Acceleration spectrum intensity, ASI
13	Velocity spectrum intensity, VSI
14	Spectral acceleration, Sa (T = 0.4s, 5%)
15	Spectral acceleration, Sa (T = 0.6s, 5%)
16	Spectral acceleration, Sa (T = 0.8s, 5%)
17	Spectral acceleration, Sa (T = 1.8s, 5%)

Fig. 14 shows the variation of the seismic compression ratio with the direction angle of the RSN145 and RSN320 for different relative

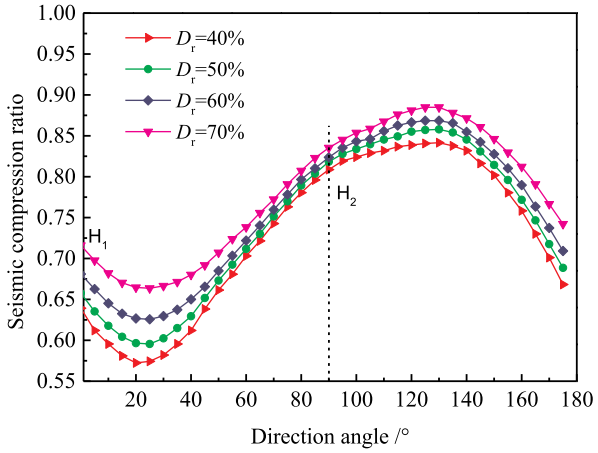

（a）RSN 145

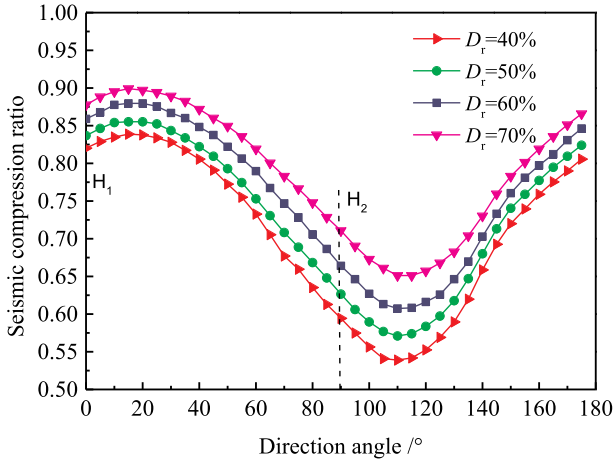

（b）RSN 320

Fig. 14. Effect of seismic directionality on seismic compression ratio with different ground motion: (a) RSN 145 and (b) RSN 320.

densities of sand. In Fig. 14H_1 and H_2 represent the horizontal directions of the original input seismic records, and the direction angles corresponding to H_1 and H_2 are 0° and 90°, respectively. As can be seen from Fig. 14, the seismic compression ratio varies significantly with the variation of the direction angle, and the maximum value of the seismic compression ratios do not correspond to the direction of H_1 and H_2, which implied that using a recorded ground motion component in the original seismic record cannot represent the effects of ground motion directionality. In addition, there is a significant discrepancy in the influence of the ground motion component at different directions on the seismic compression ratio, which indicated that the ground motion direction angle cannot quantify the seismic compression ratio. Therefore, it is unreasonable to use unidirectional seismic load to simplify bidirectional seismic load when calculating sand compression. Moreover, the seismic compression ratio decreases with the decrease of D_r when the direction angle is the same, which means the coupling of bidirectional ground motion is more significant for sand with smaller D_r values.

4.3. Correlation analysis of IM and seismic compression

To investigate the influence of relative density of sand and ground motion intensity on the seismic compression, the spectral acceleration Sa (0.6s), which has a good correlation with seismic compression, was used as the evaluation index. Sa (0.6) is the spectral acceleration of a single degree of freedom system with a natural oscillation period of 0.6 s. The relationship between seismic compression of sand with different relative densities and Sa (0.6s) in different directions of the six group ground motions is presented in Fig. 15. Each scatter in the figure represents a seismic compression induced by a ground motion in a certain direction. As can be seen from Fig. 15, the amount of seismic compression increases with the decrease of D_r, and the increase of Sa (0.6s). Saturated sand with a smaller relatively density is more prone to liquefaction and there are more pore water flows out during and after earthquake, hence resulting in a larger amount of seismic compression.

The results of the fitting relationship between the seismic compression and spectral acceleration are also shown in Fig. 15. The dispersions of the data σ, which can reflect the magnitude of the correlation between IM and seismic compression, are 0.181, 0.176, 0.174 and 0.164, respectively. It is apparent from Fig. 15 that the predictions and the σ are larger for the smaller relative density of the sand, and thus the correlation between the seismic compression and Sa (0.6s) is better with larger D_r value.

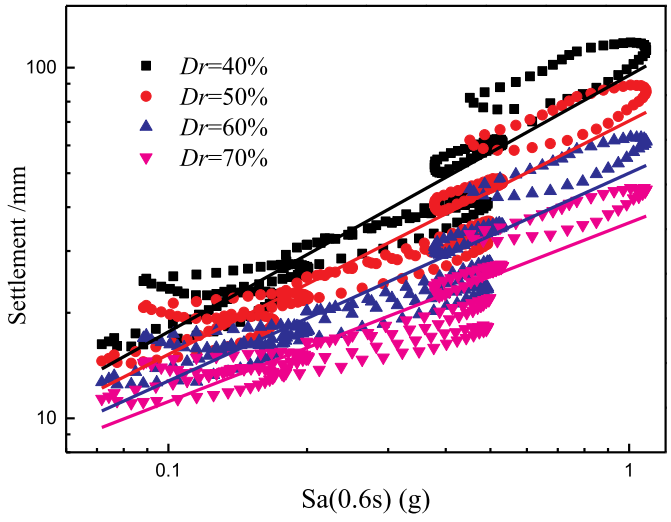

Fig. 15. Relationship between seismic compression and Sa (0.6s) for different relative density.

To further capture the relationship between ground motion intensity parameters and seismic compression, Fig. 16 summarized the dispersion of seismic compression for 17 IMs at different relative density (i.e., 40%, 50%, 60%, and 70%). As shown in Fig. 16, the dispersion is significantly affected by the relative density, which is smaller when the relative density is large. The σ corresponding to VSI (velocity spectrum intensity) and Sa (0.6s) at each relative density is less than 0.2, which indicated that the seismic compression of sand is well correlated with VSI and Sa (0.6s). However, compared with Sa (0.6s), VSI is more sensitive to the variation of relative density of sand, and it can better reflect the influence of site characteristics. Therefore, VSI is selected as an evaluation index to calculate the seismic compression of saturated sand (SCSS). The relationship between the amount of seismic compression and VSI can be expressed as Eqs. 13–16 when D_r is 40%, 50%, 60% and 70%, respectively.

$$\ln(SCSS) = 1.016\ln(VSI) + 3.132,\quad \sigma = 0.191 \tag{13}$$

$$\ln(SCSS) = 0.938\ln(VSI) + 2.832,\quad \sigma = 0.167 \tag{14}$$

$$\ln(SCSS) = 0.853\ln(VSI) + 2.514,\quad \sigma = 0.140 \tag{15}$$

$$\ln(SCSS) = 0.750\ln(VSI) + 2.054,\quad \sigma = 0.117 \tag{16}$$

It can be deduced from Eqs. 13–16 that the relationship between seismic compression and VSI satisfied the following relationship:

$$\ln(SCSS) = a\ln(VSI) + b \tag{17}$$

Considering that the fitting parameters a, b are related to the relative density, the relationship between the parameters a, b and the relative density is established, as shown in Fig. 17. It can be seen from Fig. 17 that the parameters a and b decrease with increasing of the relative density, which can be estimated according to the fitting Eqs. (18) and (19):

$$a = -0.88D_r + 1.37 \tag{18}$$

$$b = -3.55D_r + 4.59 \tag{19}$$

Combining Eqs. (17)–(19), the seismic compression can be directly predicted by D_r and VSI, where D_r reflects the characteristics of the sand field and VSI reflects the strength characteristics of the ground motion.

The proposed prediction equation was used to estimate the settlements of saturated sand deposits at the river site in the city of Niigata, Japan during the 1964 earthquake. The location of the river site and the geological survey information were detailed in Ref. [41]. A formulation given by Ishihara and Yoshimine [41] was used to calculate relative

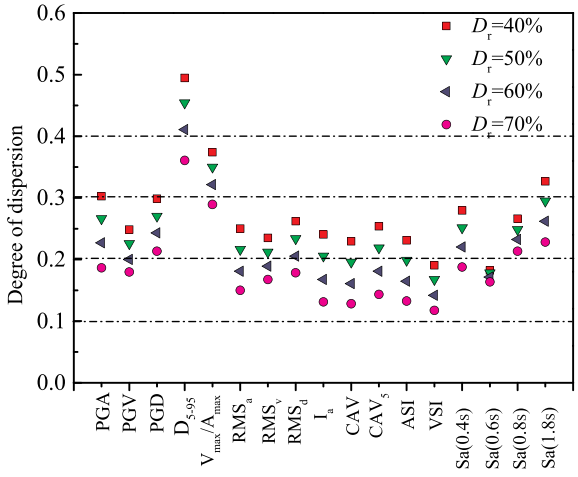

Fig. 16. Dispersion of seismic compression for 17 IMs at different relative density (i,e., 40%, 50%, 60%, and 70%).

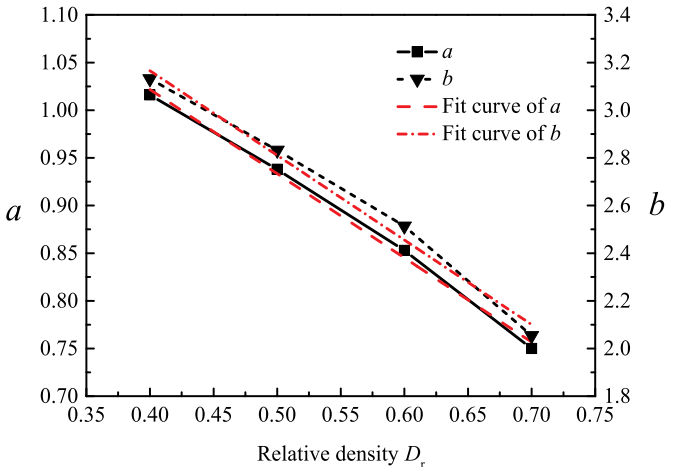

Fig. 17. Fitting curves of parameters a and b with relative density of sand.

density D_r, which can be expressed as Eq. (20):

$$D_r = 16\sqrt{N_1} \tag{20}$$

where N_1 represents the N-value in the standard penetration test corresponding to 1 kgf/cm^2 overburden pressure. The values of N_1 have been given in Ref. [41].

Fig. 18 shows the comparison of the volumetric strain reported by Ishihara and Yoshimine [41] and the values predicted in this work. As can be seen from Fig. 18, the two volumetric strain values are in good agreement in the medium sand layer and coarse sand layer, while they are significantly different in the fine sand layer and silt layer. The reason maybe that the variable permeability coefficient model and constitutive model used in this study are more suitable for the clean sand. It should be also noticed that the proposed relationships are valid for Fujian sand only, for other types of sand the results should be used with care.

5. Conclusions

Based on the variable permeability coefficient model, a seismic response analysis of free-field sites consisting of saturated Fujian sand was carried out on OpenSees platform. The influence of permeability coefficient on liquefaction-induced seismic compression was analyzed and the suitable permeability model parameters for Fujian sand were proposed to improve the accuracy of numerical test. Particular attention has been paid to the behavior of ground motion intensity measures and its relation to seismic compression, as well as the effect of relative density on the site response. On this basis, a predictive function for the seismic compression of saturated sand was proposed. The main conclusions are summarized as follows.

(1) Compared with the constant permeability coefficient model, the variable permeability model used in this study significantly improved the accuracy of numerical simulation of the seismic response (excess pore water pressure and compression) of saturated sand. For sands with different properties or drainage conditions, the permeability will be different and the parameters should be determined according to specific conditions.

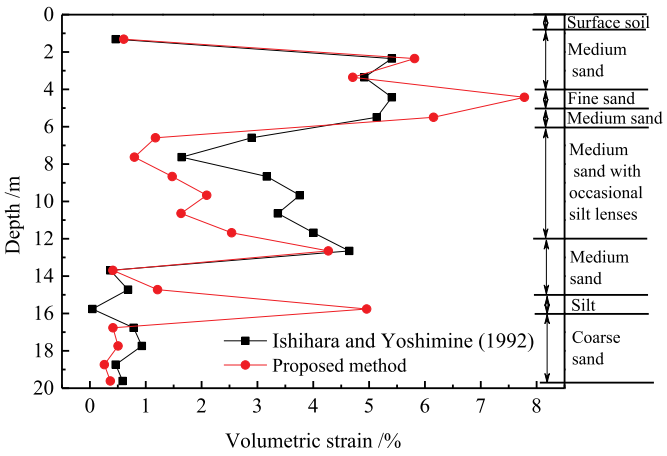

Fig. 18. Comparison of the volumetric strain for saturated soil.

(2) The ground motion direction plays a significant effect on seismic compression of saturated sand. Selecting a certain direction angle of ground motion component cannot accurately evaluate the characteristic of ground motion intensity. The pore pressure and seismic compression of saturated sand under the bidirectional load of ground motion are larger than that under unidirectional horizontal seismic load, but they are less than the sum of the results of two unidirectional loads and two times of the result of unidirectional loading. It is unreasonable to use unidirectional seismic load to simplify bi-directional seismic load to evaluate seismic compression.

(3) The seismic compression is closely related with the ground motion intensity parameter VSI, and a predictive function was proposed to estimate the compression under multi-directional seismic loadings based on the parameter of VSI and relative density of sands.

Declaration of competing interest

The authors declared that they have no conflicts of interest to this work.

We declare that we do not have any commercial or associative interest that represents a conflict of interest in connection with the work submitted.

Acknowledgments

The work described in this paper was supported by the National Natural Science Foundation of China (Project number: 41372271).

Appendix A. Supplementary data

Supplementary data to this article can be found online at https://doi.org/10.1016/j.soildyn.2019.105971.

NotationThe following symbols are used in this paper:

$a_{ROT}(t; \varphi)$ seismic acceleration component in the φ direction
$a_1(t)$, $a_2(t)$ two orthogonal acceleration time history in horizontal direction of the original seismic record, respectively
a, b model parameters related to the relative density
C a parameter related to soil properties

C_c	coefficient of curvature
C_u	coefficient of uniformity
D	total dilatancy rate
D_r	relative density
D_{50}	mean grain size;
D_{30}	medain grain size;
D_{10}	effective grain size;
d_{ir}, $\boldsymbol{\alpha}$, $\gamma_{d,r}$	irreversible dilatancy parameters
$d_{re,1}$, $d_{re,2}$	reversible dilatancy parameters
e	current void ratio
e_0	void ratio at $P_c = 0$
e_c	critical void ratio corresponding to the existing confining stress
e_{max}	maximum void ratio
e_{min}	minimum void ratio
$f_c(\sigma)$	failure surface model formulation
$f_m(\sigma)$	maximum stress ratio surface model formulation
$f_d(\sigma)$	dilatancy surface model formulation
G	elastic shear modulus
G_0, n, κ	modulus parameters
G_s	specific gravity
$g(\theta)$	plastic potential function
H	plastic modulus
h	a model parameters
$\mathbf{I}$	Identity tensor of rank 2 (Kronecker delta)
K	bulk modulus
k	permeability coefficient
k_0	initial coefficient of permeability
L	plastic loading intensity
$\mathbf{M}$	deviatoric strain flow direction
M	critical stress ratio
M_d	peak mobilized stress ratio at triaxial compression
M_m	historical maximum stress ratio
m	a parameter of the empirical index
n^b	plastic modulus parameter
n^p	a model constant
P_{at}	the standard atmospheric pressure
P_c	existing confining stress
p'	mean effective stress
q	deviatoric stress invariant
$\mathbf{r}$	the deviatoric stress ratio tensor
r_u	excess pore water pressure ratio
$\mathbf{s}$	deviatoric stress tensor
Sa(0.6)	spectral acceleration of a single degree of freedom system with a natural oscillation period of 0.6 s
SCSS	seismic compression of saturated sand;
t	time variable
VSI	velocity spectrum intensity
α, β_1, β_2	model parameters
$\boldsymbol{\alpha}_{\mathbf{in}}$	projection center
$\boldsymbol{\varepsilon}$	strain tensor
ε_v	total volumetric strain
ε_v^e	elastic volumetric strain
ε_v^p	plastic volumetric strain
ε_{vc}	volumetric strain caused by the mean effective stress
ε_{vd}	volumetric strain caused by dilatancy
$\varepsilon_{vd,ir}$, $\varepsilon_{vd,re}$	irreversible and reversible parts of ε_{vd}
η	generalized shear stress ratio
θ	the Lode angle
λ_c,ξ	model parameters
$\rho\overline{\rho}$	mapping distances in stress ratio space
$\boldsymbol{\sigma}$	effective stress tensor
φ	direction angle
ϕ	internal friction angle
ψ	state parameters

References

[1] Andrianopoulos KI, Papadimitriou AG, Bouckovalas GD. Bounding surface plasticity model for the seismic liquefaction analysis of geostructures. Soil Dyn Earthq Eng 2010;30(10):895–911.

[2] Wang R, Zhang JM, Wang G. A unified plasticity model for large post- liquefaction shear deformation of sand. Comput Geotech 2014;59(3):54–66.

[3] Elgamal A, Yang Z, Parra E, Ragheb A. Modeling of cyclic mobility in saturated cohesionless soils. Int J Plast 2003;19(6):883–905.

[4] Boulanger RW, Ziotopoulou K. Formulation of a sand plasticity plane-strain model for earthquake engineering applications. Soil Dyn Earthq Eng 2013;53(5):254–67.

[5] Zhang JM, Wang G. Large post-liquefaction deformation of sand, part I: physical mechanism, constitutive description and numerical algorithm. Acta Geotech 2012; 7(2):69–113.

[6] Jafarzadeh F, Yanagisawa E. Settlement of sand models under unidirectional shaking. In: Ishihara K, editor. First international conference on earthquake geotechnical engineering. IS-Tokyo; 1995. p. 693–8.

[7] Arulanandan K, Sybico J. Post-liquefaction settlement of sands. In: Proc. Of the wroth memorial symp. St. Catherine's College, Oxford, UK, London, UK: Thomas Telford; 1993. p. 94–110.

[8] Shahir H, Pak A, Taiebat Jeremić B. Evaluation of variation of permeability in liquefiable soil under earthquake loading. Comput Geotech 2012;40(3):74–88.

[9] Shahir H, Mohammadi HB, Ghassemi A. Employing a variable permeability model in numerical simulation of saturated sand behavior under earthquake loading. Comput Geotech 2014;55(1):211–23.

[10] Rahmani A, Ghasemi FO, Pak A. Investigation of the influence of permeability coefficient on the numerical modeling of the liquefaction phenomenon. Sci Iran 2012;19(2):179–87.

[11] Ueng TS, Wu CW, Cheng HW, Chen CH. Settlements of saturated clean sand deposits in shaking table tests. Soil Dyn Earthq Eng 2010;30(1):50–60.

[12] Bradley BA, Baker JW. Ground motion directionality in the 2010–2011 Canterbury earthquakes. Earthq Eng Struct Dyn 2014;44(3):371–84.

[13] Nie CX, Chen QS, Gao GY, Yang J. Determination of seismic compression of sand subjected to two horizontal components of earthquake ground motions. Soil Dyn Earthq Eng 2017;92:330–3.

[14] Boore DM. Orientation-independent, nongeometric-mean measures of seismic intensity from two horizontal components of motion. Bull Seismol Soc Am 2010; 100(4):1830–5.

[15] García F, Aznárez JJ, Padrón LA, Maeso O. Relevance of the incidence angle of the seismic waves on the dynamic response of arch dams. Soil Dyn Earthq Eng 2016; 90:442–53.

[16] Song J, Gao YF, Adrian RM, Feng TG. Empirical predictive relationships for rigid sliding displacement based on directionally-dependent ground motion parameters. Eng Geol 2017;222:124–39.

[17] Song J, Wu KL, Gao YF, Feng TG. Influence of interactions between topographic and soil layer amplification on seismic response of sliding mass and slope displacement. Soil Dyn Earthq Eng 2020. https://doi.org/10.1016/j.soildyn.2019.105901.

[18] Ishihara K, Yasuda S. Sand liquefaction under random earthquake loading condition. In: Proceeding of 5th WCEE. Canda; 1973. p. 329–38.

[19] Riddell R, Eeri AM. On ground motion intensity indices. Earthq Spectra 2007;23 (1):147–73.

[20] Athanatopoulou AM, Tsourekas A, Papamanolis G. Variation of response with incident angle under two horizontal correlated seismic components. Earthquake Resistant Engineering Structures V 2014;81(5):183–92.

[21] Shahnazari H, Towhata I. Torsion shear tests on cyclic stress-dilatancy relationship of sand. Soils Found 2002;42(1):105–19.

[22] Whang DH, Stewart JP. Effect of compaction conditions on the seismic compression of compacted fill soils. Geotech Test J 2004;27(4):371–9.

[23] Stamatopoulos CA, Balla LN, Stamatopoulos AC. Earthquake-induced settlement as a result of densification, measured in laboratory tests. In: Proc. 13th world conf on earthq eng. Vancouver; 2004. p. 1–15.

[24] Pyke R, Seed HB, Chan CK. Settlement of sands under multidirectional shaking. ASCE J. Geot Eng Div 1975;101(4):379–98.

[25] Tokimatsu K, Seed HB. Evaluation of settlements in sands due to earthquake shaking. J Geotech Engrg 1987;113(8):861–78.

[26] Duku PM, Stewart JP, Whang DH, Yee E. Volumetric strains of clean sands subject to cyclic loads. ASCE J. Geot Eng Div 2008;134(8):1073–85.

[27] Ghayoomi M, McCartney JS, Ko HY. An empirical methodology to estimate seismically induced settlement of partially saturated sand. ASCE J. Geot Eng Div 2013;139(3):367–76.

[28] Lasley SJ, Green RA, Chen QS, Rodriguez-Marek A. Approach for estimating seismic compression using site response analyses. ASCE J. Geot Eng Div 2016;142 (6):04016015.

[29] Cornell CA, Krawinkler H. Progress and challenges in seismic performance assessment. PEER Cent News 2000;20(2):130–9.

[30] Dafalias YF, Popov EP. A model of nonlinearly hardening materials for complex loading. Acta Mech 1975;21(3):173–92.

[31] Been K, Jefferies MG. A state parameter for sands. Geotechnique 1985;35(2): 99–112.

[32] Power M, Chiou B, Abrahamson N, Bozorgnia Y, Shantz T, Roblee C. An overview of the NGA project. Earthq Spectra 2008;24(1):3–21.

[33] Liang T. Characterizing liquefaction resistance of clayey sand by shear wave velocity. Hangzhou: Dissertation of Zhejiang University (Tutor: Yanguo Zhou); 2013 [In Chinese)].

[34] Taylor DW. Fundamentals of soil mechanics. New York: John Wiley and Sons Inc; 1948.

[35] Phillips C, Hashash YMA, Olson SM, et al. Significance of small strain damping and dilation parameters in numerical modeling of free-field lateral spreading centrifuge tests. Soil Dyn Earthq Eng 2012;42:161–76.

[36] Yang Z, Lu J, Elgamal A. OpenSees soil models and solid-fluid fully coupled elements (User's Manual). San Diego: University of California; 2008.

[37] Kayen RE, Mitchell JK. Assessment of liquefaction potential during earthquakes by Arias intensity. J Geotech Geoenviron Eng 1997;123(12):1162–74.

[38] Kramer SL, Mitchell RA. Ground motion intensity measures for liquefaction hazard evaluation. Earthq Spectra 2006;22(2):413–38.

[39] Kramer SL, Arduino P, Shin H. Using OpenSees for performance-based evaluation of bridges on liquefiable soils. Pacific Earthquake Engineering Research Center; 2008.

[40] Bradley BA, Cubrinovski M, Dhakal RP, MacRae GA. Intensity measures for the seismic response of pile foundations. Soil Dyn Earthq Eng 2009;29(6):1046–58.

[41] Ishihara K, Yoshimine M. Evaluation of settlements in sand deposits following liquefaction during earthquake. Soils Found 1992;32(1):173–88.